Use of a Pro-Fibrogenic Mechanism-Based Predictive Toxicological Approach for Tiered Testing and Decision Analysis of Carbonaceous Nanomaterials

Xiang Wang,[†,‡] Matthew C. Duch,[§] Nikhita Mansukhani,[§] Zhaoxia Ji,[‡] Yu-Pei Liao,[†] Meiying Wang,[†] Haiyuan Zhang,[‡] Bingbing Sun,[†] Chong Hyun Chang,[‡] Ruibin Li,[†] Sijie Lin,[‡] Huan Meng,[†,‡] Tian Xia,[†,‡] Mark C. Hersam,[§] and André E. Nel*[,†,‡]

[†]Division of NanoMedicine, Department of Medicine; [‡]California NanoSystems Institute, University of California, Los Angeles, California 90095, United States and [§]Departments of Materials Science and Engineering, Chemistry, and Medicine, Northwestern University, Evanston, Illinois 60208, United States

ABSTRACT Engineered carbonaceous nanomaterials (ECNs), including single-wall carbon nanotubes (SWCNTs), multiwall carbon nanotubes (MWCNTs), graphene, and graphene oxide (GO), are potentially hazardous to the lung. With incremental experience in the use of predictive toxicological approaches, seeking to relate ECN physicochemical properties to adverse outcome pathways (AOPs), it is logical to explore the existence of a common AOP that allows comparative analysis of broad ECN categories. We established an ECN library comprising three different types of SWCNTs, graphene, and graphene oxide (two sizes) for comparative analysis according to a cell-based AOP that also plays a role in the pathogenesis of pulmonary fibrosis. SWCNTs synthesized by Hipco, arc discharge and Co—Mo catalyst (CoMoCAT) methods were obtained in their as-prepared (AP) state, following which they were further purified (PD) or coated with Pluronic F108 (PF108) or bovine serum albumin (BSA) to improve dispersal and colloidal stability. GO was prepared as two sizes, GO-small (S) and GO-large (L), while the graphene samples were coated with BSA and PF108 to enable dispersion in aqueous solution. *In vitro* screening showed that AP- and PD-SWCNTs, irrespective of the method of synthesis, as well as graphene (BSA) and GO (S and L) could trigger interleukin-1β (IL-1β) and transforming growth factor-β1 (TGF-β1) production in myeloid (THP-1) and epithelial (BEAS-2B) cell lines, respectively. Oropharyngeal aspiration in mice confirmed that AP-Hipco tubes, graphene (BSA-dispersed), GO-S and GO-L could induce IL-1β and TGF-β1 production in the lung in parallel with lung fibrosis. Notably, GO-L was the most pro-fibrogenic material based on rapid kinetics of pulmonary injury. In contrast, PF108-dispersed SWCNTs and -graphene failed to exert fibrogenic effects. Collectively, these data indicate that the dispersal state and surface reactivity of ECNs play key roles in triggering a pro-fibrogenic AOP, which could prove helpful for hazard ranking and a proposed tiered testing approach for large ECN categories.

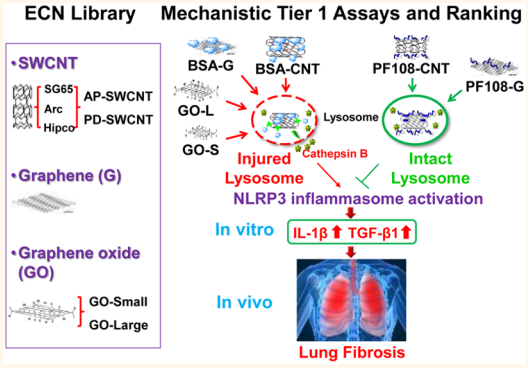

KEYWORDS: engineered carbonaceous nanomaterials · SWCNT · graphene · graphene oxide · NLRP3 inflammasome lung fibrosis

Engineered carbonaceous nanomaterials (ECN), including carbon nanotubes (CNTs), graphene, and graphene oxide (GO), have been shown to be capable of inducing lung injury.[1−8] For instance, single-walled (SW) and multiwalled carbon nanotubes (MWCNTs) generate acute lung injury as well as subchronic granulomatous inflammation and fibrosis in the rodent lung, whether through intratracheal instillation or aerosolized inhalation.[1−4] Similarly, graphene and GO are capable of inducing pulmonary inflammation and fibrosis.[5−8] However, in spite of overlapping properties and the ability to cause qualitatively similar lung damage, these materials differ significantly with respect to shape, aspect ratio, electronic properties and surface reactivity, begging the question as to whether there is a common adverse outcome pathway (AOP) on which to base structure—activity relationships (SARs) that can be used to

* Address correspondence to anel@mednet.ucla.edu.

Received for review December 18, 2014 and accepted February 3, 2015.

Published online February 03, 2015
10.1021/nn507243w

categorize materials based on lung fibrosis potential. Moreover, previous investigation of the hazard potential of SWCNTs has predominantly explored tubes synthesized by one of the major synthesis methods, without direct comparison of how different levels of catalyst impurities, tube dimensions, aspect ratios or structural defects of tubes synthesized by gas phase decomposition of CO (Hipco), electric arc discharge, or silica-supported Co−Mo catalyst (CoMoCAT) may contribute to lung injury.[9] Also, no systematic study has been undertaken to directly compare graphene with CNTs based on shared or different physicochemical properties, including the possibility that a common AOP could emerge for hazard ranking and material comparisons that can be instructive for regulatory decision-making.

We have previously demonstrated that MWCNTs can trigger pro-fibrogenic responses in cells and the intact rodent lung, which allows a comparative analysis for a large number of materials in one assessment, of how dispersion, hydrophobicity, surface functionalization, surface coating and bioavailability contribute to hazard potential.[3,10−12] These studies demonstrated that better dispersed MWCNTs are more prone toward inducing interleukin-1β (IL-1β) and transforming growth factor-β1 (TGF-β1) production in macrophages and epithelial cells, respectively. Alveolar epithelial cells and macrophages constitute a trophic cellular unit in which intercellular communication through cytokines and growth factors plays a key role in the pathogenesis of pulmonary fibrosis.[13] Triggering of IL-1β production in macrophages results from tube damage to lysosomes, leading to the assembly of the NLRP3 (NOD-like receptor family, pyrin domain containing 3) inflammasome, which is responsible for converting pro-IL-1β to IL-1β.[10,11] IL-1β acts in synergy with epithelial produced TGF-β1 to promote epithelial-mesenchymal transition, which cumulates in the formation of fibroblast-like cells that deposit collagen in the lung.[14] This march of events presents us with a series of molecular biomarkers that can be tracked at cellular and organ level to establish a predictive toxicological paradigm, which can be used to compare the hazard potential of large batches of ECNs other than MWCNTs.[13] This knowledge could be of potential use to establish structure−activity relationships for grouping, ranking and risk assessment of a wide range of ECNs, with the ability to establish decision trees for further testing requirements.

In this study, we established an ECN library comprised of three different types of SWCNTs as well as graphene and GO for comparative analysis and identification of overlapping and unique physicochemical properties that trigger lung fibrosis. We demonstrate that the state of dispersion and the type of dispersant (*e.g.*, BSA *vs* Pluronic F108) play major roles in the pro-fibrogenic effects of SWCNTs, irrespective of the method of synthesis, impurities, or length of these materials. We also show that the dispersal state and surface functionalization play major roles in determining the toxicological potential of ECNs in the mouse lung. The relationship of these properties to a common AOP could prove helpful for establishing provisional SARs, which can be used to formulate further testing strategies of a broad range of ECNs according to a tiered approach that we will propose.

RESULTS

Characterization of SWCNT, Graphene, and Graphene Oxide. We established an ECN library composed of SWCNTs, graphene, and GO to perform a comparative analysis of physicochemical properties that could lead to pulmonary fibrosis. All materials were comprehensively characterized as shown in Figure 1 and Tables 1 and 2. SWCNTs were synthesized according to the Hipco, arc discharge (Arc) and CoMoCAT (SG65) methods. The as-prepared (AP) tubes were further purified (PD) by acid treatment to reduce impurity levels (with the exception of SG65-SWCNTs supplied in purified format only). While TEM analysis did not show obvious structural differences in the tubes synthesized by the 3 different methods (Figure 1A), ICP-MS analysis revealed differences for the metal impurities (Table 1A). Thus, AP-Hipco tubes had a Fe content of 31%, which decreased to 16% after purification. PF108 surface coating and centrifugational harvesting further decreased the Fe content to 6.5%. Similarly, the Y and Ni contents of electric arc discharge tubes decreased from 11.91% and 32.71%, respectively, to 0.55% and 1.60% after purification. These amounts decreased to 0.06% and 0.15% after PF108 coating. Purified CoMoCAT tubes had Co and Mo contents of 0.65% and 4.73%, respectively, which decreased to 0.22% and 1.58% after PF108 dispersion. Following dispersion in DI H_2O, the hydrodynamic sizes of AP and PD Hipco tubes were 1218 and 584 nm, respectively, which decreased to 272 nm after PF108 coating. PF108 coating also decreased the bundle diameter from 10 nm to less than this size. Similar trends could be seen in Arc and CoMoCAT tubes (Table 1A). It should be noted that the PF108 coating procedure involves ultrasonication, which reduces the average size of the carbon nanomaterials, and centrifugation, removing sedimenting species, including aggregates and large catalyst particles, more quickly, thus reducing the metal content (see Materials and Methods for more details).[15,16]

Our library also included 2-dimensional, sheet-like graphene and GO flakes (Figure 1B). The primary size of the small flakes (GO-S) was 329 nm, while that of the large flakes (GO-L) was 2007 nm (Table 1B). Because of the hydrophobicity of graphene and the lack of colloidal stability in aqueous media, we used bovine serum albumin (BSA) and PF108 to improve material dispersion by surface coating. The average flake size of

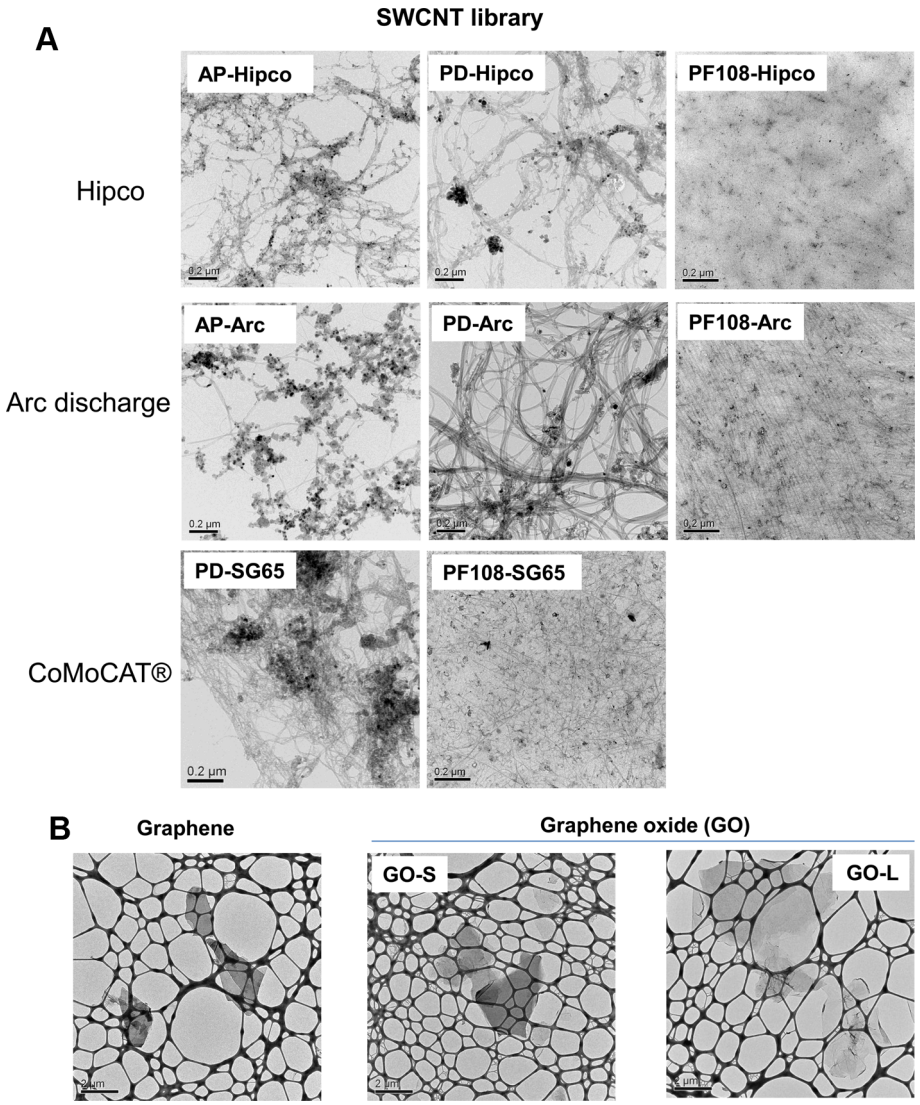

Figure 1. Representative transmission electron microscopy (TEM) images of the SWCNTs, graphene, and graphene oxide nanomaterials. TEM images were acquired using a JEOL 100 CX transmission electron microscope at 80 kV in the UCLA BRI Electron Microscopy Core. AP, as prepared; PD, purified; PF108, PF108-dispersed.

TABLE 1. Physicochemical Characterization of SWCNTs[a]

			SWCNTs							
properties	**tools**	**unit**	**AP-Hipco**	**PD-Hipco**	**PF108-Hipco**	**AP-Arc**	**PD-Arc**	**PF108-Arc**	**PD-SG65**	**PF108-SG65**
Tube diameter	UV−vis	nm	0.7−1.1	0.7−1.1	0.7−1.1	1.2−2.0	1.2−2.0	1.2−2.0	0.7−1.0	0.7−1.0
Bundle diameter	TEM	nm	10.7 ± 3.6	13.0 + 3.5	5.0−10.0	6.3 ± 2.0	7.5 ± 2.4	∼5.0	7.4 ± 2.3	∼5.0
Length	TEM/AFM	μm	1000−5000	500−1500	500−1500	100−1000	100−1000	100−1000	450−2000	450−2000
Metal Impurity	ICP-MS	%	31.35	16.01	6.52	11.91 ± 32.71	0.55 ± 1.60	0.06 ± 0.15	0.65 ± 4.73	0.22 ± 1.58
				Fe			Y + Ni		Co + Mo	
ζ potential in H_2O	ZetaPALS	mV	−22.3 ± 0.7	−39.9 ± 2.7	−10.4 ± 1.8	−25.4 ± 0.7	−29.3 ± 2.4	−6.3 ± 1.1	−23.4 ± 1.0	−9.0 ± 0.6
Size in H_2O	DLS	nm	1218 ± 507	584 ± 180	272 ± 26	880 ± 175	644 ± 206	150 ± 23	458 ± 128	154 ± 32
Size in BEGM	DLS	nm	1157 ± 20	681 ± 46	122 ± 2	974 ± 14	566 ± 35	121 ± 2	327 ± 5	169 ± 6
Size in RPMI	DLS	nm	920 ± 45	639 ± 25	78 ± 1	836 ± 23	602 ± 15	79 ± 1	305 ± 4	97 ± 2

[a] The average lengths and diameters of the tubes were assessed by UV−vis and TEM microscopy (JEOL 100 CX transmission electron microscope). The elemental composition was determined by ICP-MS. The zeta potential was measured using a ZetaSizer Nano-ZS (Malvern Instruments, Worcestershire WR, U.K.). The hydrodynamic diameters in H_2O, BEGM and RPMI were determined using high-throughput dynamic light scattering (HT-DLS, Dynapro Plate Reader, Wyatt Technology). AP, as prepared; PD, purified; PF108, Pluronic F108.

TABLE 2. Physicochemical Characterization of Graphene and Graphene Oxide[a]

			graphene		graphene oxide	
properties	technique	unit	G	PF108-G	GO-S	GO-L
Diameter	TEM/AFM	nm	640	45	179	1676
ζ potential in H_2O	ZetaPALS	mV	-27.1 ± 0.6	-8.7 ± 0.8	-30.9 ± 2.7	-14.8 ± 1.6
Size in H_2O	DLS	nm	1179 ± 109	236 ± 19	330 ± 28	2007 ± 136
Size in BEGM	DLS	nm	744 ± 124	128 ± 10	2368 ± 264	3432 ± 394
Size in RPMI	DLS	nm	1036 ± 247	109 ± 10	629 ± 38	2134 ± 314

[a] The average diameter of the graphene and graphene oxide were assessed by UV—vis and TEM microscopy (JEOL 100 CX transmission electron microscope). The elemental composition was determined by ICP-MS. The zeta potential was measured using a ZetaSizer Nano-ZS (Malvern Instruments, Worcestershire WR, U.K.). The hydrodynamic diameters in H_2O, BEGM and RPMI were determined using high-throughput dynamic light scattering (HT-DLS, Dynapro Plate Reader, Wyatt Technology). BSA, bovine serum albumin; G, graphene; PF108:,Pluronic F108; GO, graphene oxide; S, small; L, large.

graphene decreased from 640 to 45 nm after FP108 coating (Table 1B). After aqueous suspension, the hydrodynamic sizes of the BSA and PF108 coated graphene yielded agglomerated flakes of sizes 1179.2 and 236.3 nm, respectively. GO-S and GO-L were generated by varying the sonication power output, resulting in flake sizes of 179 and 1676 nm, respectively. No dispersant was needed for GO, which is hydrophilic in nature. However, when performing the cellular studies, GO may interact with BSA in the cell culture medium but were not deliberately applied as a coat. The zeta potentials of these materials were in the range of -8.7 to -30.9 mV in distilled water. The hydrodynamic sizes for GO-S and GO-L were 239.9 and 2007.8 nm, respectively.

Comparison of ECN Materials for Their Abilities To Induce Lysosomal Damage and IL-1β Production in THP-1 Cells. We used the monocytic-derived cell line, THP-1, to assess NLRP3 inflammasome activation and IL-1β production as previously described.[11,13] Assessment of cell viability showed that only BSA-dispersed AP- and PD-SWCNTs showed a significant decline of cellular viability (as determined by MTS and LDH assays) at relatively high concentrations >50 μg/mL (Supporting Information Figure S1A,B). In contrast, all PF108-dispersed materials and GO failed to exhibit cytotoxicity (Supporting Information Figure S1A,B). Assessment of IL-1β levels in the culture supernatants showed that AP- and PD-SWCNTs (BSA-coated), graphene and BSA-dispersed GO induced significant increases above the nontreated control, while PF108-dispersed tubes and graphene showed little or no effect (Figure 2A,B). Both the cell viability and cytokine data are correlated to the suspension (colloidal) stability of these materials, with the PF108-dispersed SWCNTs eliciting significantly less IL-1β production compared to BSA-dispersed AP- and PD-tubes (Figure 2A and Supporting Information Figure S1A,B). This is in agreement with the enhanced suspension stability of PF108 *vs* BSA-coated tubes (Supporting Information Figure S2). Moreover, PF108-coating also had improved the colloidal stability of graphene compared to the BSA-coated material. The decreased sedimentation rate of PF108-coated graphene flakes was accompanied by decreased cytotoxicity and IL-1β production, likely as a result of decreased cellular exposure at the bottom of the dish. Suspension stability affects the bioavailability and the cellular uptake of ECN materials in THP-1 cells as determined by side scatter analysis (Supporting Information Figure S3). This demonstrated that all the materials except for PF108-coated graphene are taken up in THP-1 cells and are capable of inducing IL-1β production.

Because NLRP3 inflammasome activation by MWCNTs requires lysosomal damage and cathepsin B release,[3,11] we used a fluorescent cathepsin B substrate, Magic Red, to study lysosome integrity and enzyme release by confocal microscopy. This demonstrated that BSA-dispersed AP and PD tubes of the Hipco variety, BSA-graphene (BSA-G), GO-S and GO-L could induce lysosomal damage and the cytosolic release of cathepsin B (Figure 2C). In contrast, PF108-dispersed tubes and graphene did not result in lysosome damage, as demonstrated by the speckled fluorescence of Magic Red in the intact organelle. Similarly, BSA-dispersed AP and PD tubes obtained by Arc discharge or PD tubes obtained through CoMoCAT synthesis, induced lysosome damage, while PF108-coated tubes had no effect on the lysosome (data not shown). All considered, the confocal data agrees with IL-1β profiles, confirming that lysosome damage is instrumental in generating the NLRP3-mediated inflammatory responses.

Comparison of the ECN Materials for Their Ability To Induce TGF-β1 Production in BEAS-2B Cells. Because TGF-β1 production by alveolar epithelial cells contributes to the pathogenesis of pulmonary fibrosis (in synergy with IL-1β), we assessed TGF-β1 levels in the supernatant of the transformed human lung epithelial cell line, BEAS-2B. Although none of the ECN materials impacted BEAS-2B cell viability (Supporting Information Figure S4A,B), the BSA-coated AP- and PD-SWCNTs, BSA-coated graphene and both types of GO induced significant TGF-β1 production (Figure 3A and B). GO-L induced a more robust response (Figure 3B).

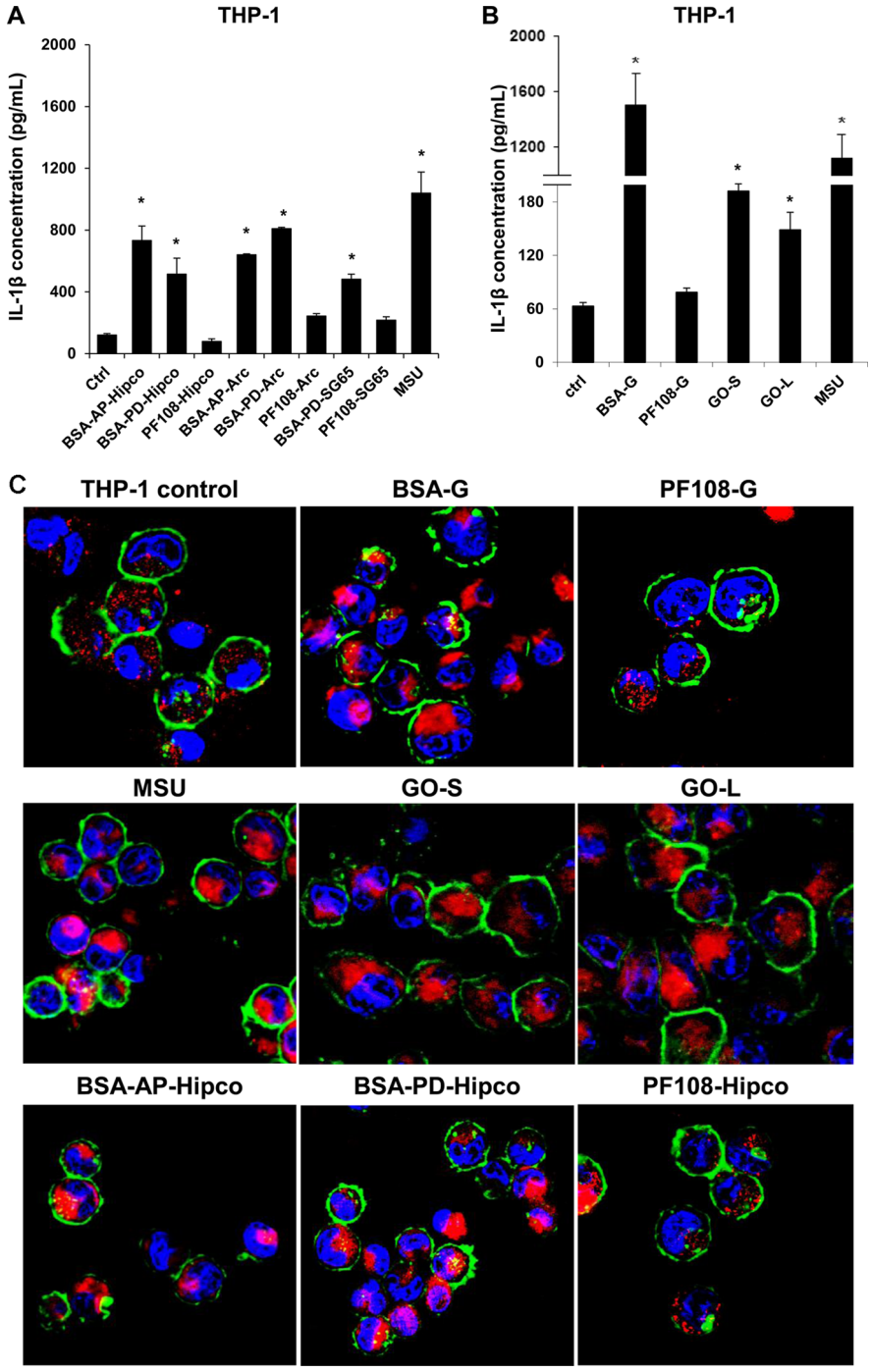

Figure 2. Comparative pro-fibrogenic effect of SWCNTs, graphene (G) and graphene oxide (GO) ECNs, as reflected by IL-1β production and NLRP3 inflammasome activation in THP-1 cells. IL-1β levels were determined by ELISA, using the supernatants of THP-1 cells treated with SWCNTs (A), graphene and graphene oxide (B) for 24 h. *$p < 0.05$ compared to control. (C) Confocal microscopy demonstrating the effects of tube coating on lysosome damage in THP-1 cells. Lysosomal damage and cathepsin B release were determined by Magic Red staining. THP-1 cells were seeded into 8-well chamber slides and incubated with 100 μg/mL AP, PD and PF108-Hipco SWCNTs, graphene and graphene oxide in complete RPMI 1640 for 24 h. After fixation and permeabilization, cells were stained with Magic Red (ImmunoChemistry Technologies), wheat germ agglutinin 633 and Hoechst 33342 dye, followed by visualization under a confocal 1P/FCS inverted microscope. Monosodium urate (MSU) crystals were used as a positive control demonstrating that the punctate Magic Red staining seen in intact lysosomes (control cells) changes to diffuse cytosolic fluorescence after damage to the lysosome.

In contrast, PF108 coating protected all of the listed ECNs from triggering TGF-β1 production (Figure 3A,B). All considered, the TGF-β1 data are in good agreement with the colloidal suspension stability index (Supporting Information Figure S2C,D) of the various materials, as discussed for IL-1β production.

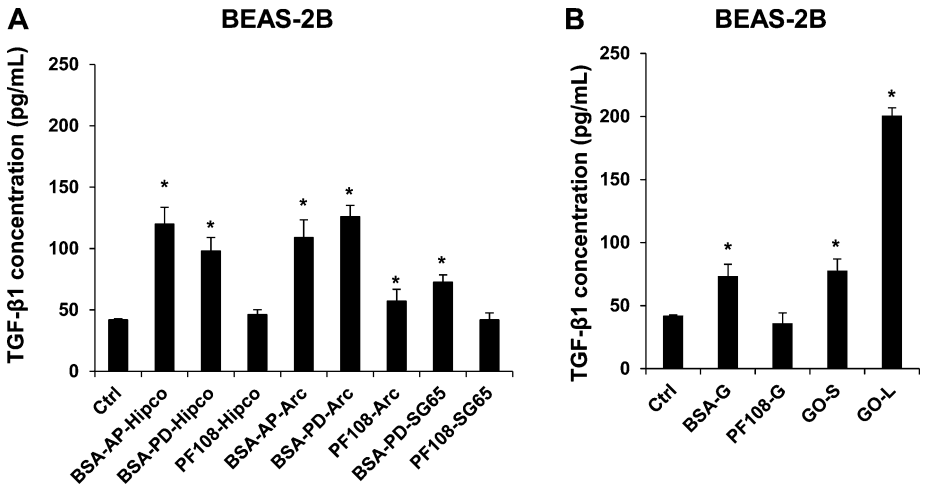

Figure 3. Comparison of the pro-fibrogenic effects of SWCNTs, graphene (G) and graphene oxide (GO) nanomaterials on TGF-β1 production in BEAS-2B cells. BEAS-2B cells were treated for 24 h with the SWCNTs, graphene and GO nanomaterials at the dose of 100 μg/mL and the supernatants were collected to measure the TGF-β1 production by ELISA. *$p < 0.05$ compared to control.

SWCNTs, Graphene, and Graphene Oxide Induce Acute Lung Inflammation in Mice. Oropharyngeal aspiration of 2 mg/kg of each of the graphene materials as well as Hipco SWCNTs was used to determine the possible effects on pulmonary inflammation in C57BL/6 mice. This dose was selected based on prior dose response studies that were undertaken on MWCNTs and SWCNTs; 2 mg/kg falls on the linear part of the dose–response curve.[3,11,17] The mice were sacrificed after 40 h to collect bronchoalveolar lavage fluid (BALF) and lung tissue. We have previously shown that IL-1β is produced within this time window in response to MWCNTs, while the production of TGF-β1 occurs over days to weeks. BALF analysis showed increased neutrophil counts and LIX (LPS-induced CXC chemokine) levels for all the materials tested, including for quartz (QTZ), which was used as a positive control (Supporting Information Figure S5A–C). The occurrence of acute inflammation was confirmed by H&E staining of lung sections, which showed mild inflammation around small- and medium-sized airways, except for the GO materials, which generated more intense inflammation, particularly GO-L (Supporting Information Figure S4D). Measurement of IL-1β levels in the BAL fluid showed that while AP-Hipco, BSA-G and GO-S induced statistically significant increases, PF108-G and GO-L did not show increased production at 40 h (Figure 4A). QTZ also induced a robust response. The apparent failure of GO-L to induce an IL-1β response was surprising in light of its robust effect in THP-1 cells (Figure 2B). This unexpected outcome prompted us to revisit the kinetics of the IL-1β production in the lung by sacrificing the animals at 6 h, 18 h, 40 h, 3 days, 7 days, and 21 days following the aspiration of GO-L, GO-S and QTZ (Figure 4). Interestingly, this experiment demonstrated high levels of IL-1β production in response to GO-L by 6 h followed by a rapid decline and a second small rise at day 3. In contrast, GO-S induced an early increase,

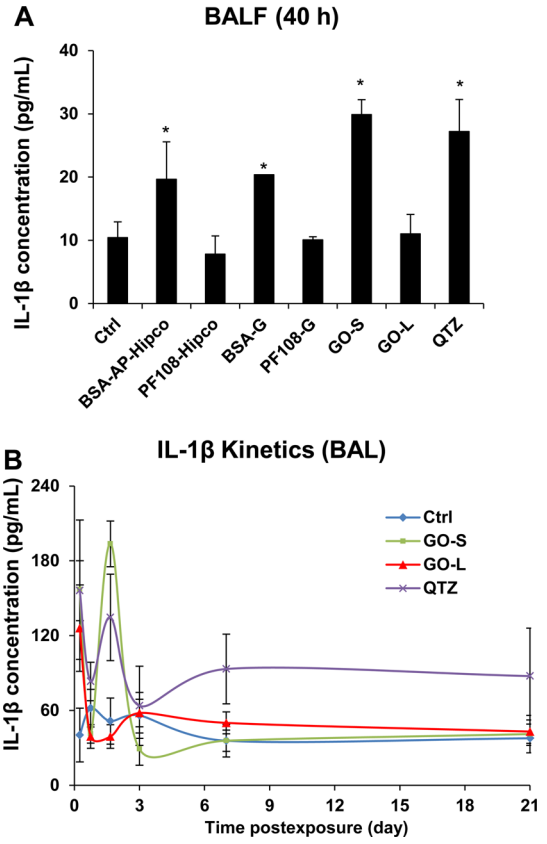

Figure 4. IL-1β production in response to bolus aspiration of ECNs, followed by acute or kinetic analysis of the BALF in mice. (A) C57BL/6 mice were exposed to Hipco-SWCNTs, graphene and graphene oxide at 2 mg/kg by oropharyngeal aspiration, followed by BALF collection after 40 h to determine IL-1β activity with an ELISA kit (n = 6 animals per group). Min-U-Sil at 5 mg/kg served as positive control. *$p < 0.05$ compared with control. (B) Kinetics experiment in which C57BL/6 mice were exposed to graphene oxide materials (2 mg/kg) and Min-U-Sil (5 mg/kg) by oropharyngeal aspiration, followed by sacrifice after 6 h, 18 h, 40 h, 3 d, 7 d, and 21 d. The BALF was collected to determine IL-1β levels by ELISA. *$p < 0.05$ compared to control. There were 6 animals in each group.

but this was accompanied by a prominent second IL-1β peak by 40 h (Figure 4B). The significant difference in the kinetics of IL-1β production by GO-L and GO-S at 40 h explains the data in Figure 4A, where 40 h after exposure to GO-L there is no evidence of increased IL-1β production. QTZ also induced two peaks of IL-1β production at 6 and 40 h, followed by prolonged cytokine elevation for up to 21 days.

Selected ECN Materials Show Differential Effects on Lung Fibrosis. We also assessed subchronic lung injury 21 days after a single oropharyngeal instillation of 2 mg/kg Hipco tubes (BSA and PF108-coated), graphene (BSA and PF108-coated), GO-L and GO-S. Although the neutrophil counts were not increased in the BALF at this time point (Supporting Information Figure S6A), H&E staining showed pulmonary infiltrates around small- and medium-sized airways for most tested materials (Supporting Information Figure S6B). GO-L exerted the most prominent effect besides QTZ. While IL-1β levels returned to baseline after 21 days (Figure 4B), AP-Hipco tubes, BSA-G, GO-S and GO-L generated significant TGF-β1 elevations (Figure 5A). In contrast, PF108-dispersed SWCNTs and graphene failed to exert similar effects (Figure 5A). The kinetics of TGF-β1 production by graphene oxide materials in the experiment described in Figure 5B showed a rise in growth factor production by 40 h, followed by a progressive rise over the next 20 days (Figure 5B). GO-L induced a more robust response than GO-S. Clear evidence of increased collagen production by AP-Hipco, BSA-G, GO-S, GO-L nanoparticles and QTZ could be demonstrated by the Sircol assay (Figure 5C) as well as the trichrome staining (blue) (Figure 5D). GO-L induced the most robust response besides QTZ, while PF108-dispersed SWCNT and PF108-dispersed graphene failed to show pro-fibrogenic effects. All considered, the 21 day study showed that all ECNs, except PF108-dispersed materials, induce pulmonary fibrosis at 2 mg/kg, with GO-L providing the strongest response. This study confirms the utility of the predictive lung fibrosis paradigm for comparative analysis and ranking of toxicological potential of the broad range of ECNs.

DISCUSSION

In this study, we compared the cellular and pulmonary responses of a library of SWCNTs and graphene materials according to a predictive paradigm that link lysosome injury and cytokine production to the pathogenesis of pulmonary fibrosis. We demonstrate that in spite of the differences in the physicochemical properties of the SWCNTs and graphene flakes in terms of size, shape, metal content, and colloidal stability, all the materials are capable of triggering NLRP3 inflammasome activation, IL-1β and TGF-β1 production and lung fibrosis, with variable levels of injury. GO-L induced the most pronounced pro-fibrogenic effects. Coating of graphene and SWCNTs with PF108 decreased their pro-fibrogenic potential, demonstrating the importance of ECN surface reactivity in determining bioavailability and lysosomal injury as key ingredients of a lysosome/inflammasome-injury pathway in the lung. All considered, these data demonstrate the utility of a predictive toxicological paradigm for SWCNTs and graphene (in addition to MWCNTs), and show lysosome damage and NRLP3 inflammasome activation can be used as a final common pathway for ranking of the lung fibrosis potential of a wide range of ECNs. This ranking can be used toward a tiered decision-making process for the safety testing of ECNs.

Although it has been shown that the presence of SWCNT metal impurities can play a role in cytotoxicity and acute pulmonary and cardiovascular responses,[18,19] we did not observe a major impact on cell viability outcome during the purification and reducing the metal content of the raw tubes (Table 1A). Moreover, there were also no major differences between the raw and purified tubes in terms of their abilities to trigger IL-1β and TGF-β1 production in THP-1 and BEAS-2B cells, respectively (Figures 2A and 3A). These data suggest that a tube characteristics such as a reactive carbon surface plays an important role in the pro-fibrogenic effects. This notion is further supported by the finding that PF108 coating prevents the damaging effects of SWCNT surfaces in the lysosome, leading to reduced IL-1β production. In this regard, we have recently shown that the generation of reactive oxygen species (ROS) plays a role in the catalytic injury by SWCNTs, in part through the activation of NADPH oxidase during the phagocytic uptake of these materials by macrophages.[35] This suggests that the long aspect ratio of the tubes is important for contact and wrapping by the surface membrane, where the assembled NADPH oxidase complex is incorporated into the phagosome.[35] Moreover, the space constraints in the lysosome allow close contact of the tubes with the organelle membrane, allowing the reactive surface and oxygen radical generation to deliver an injurious impact to the lysosome membrane. The combination of oxidative stress and cathepsin B release leads to NLRP3 inflammasome activation and IL-1β production.[35] This scenario could also explain the protective effect of PF108, which remains stably attached to the tube surfaces under acidic lysosomal conditions, thereby interfering in damage to the lysosomal membrane, as described for MWCNTs.[11] While it is interesting that we did not observe major differences between Hipco, Arc and CoMoCAT SWCNTs in terms of cellular pro-fibrogenic responses, it is important to explain that these synthesis methods could nonetheless contribute to a different set of biological outcomes that could

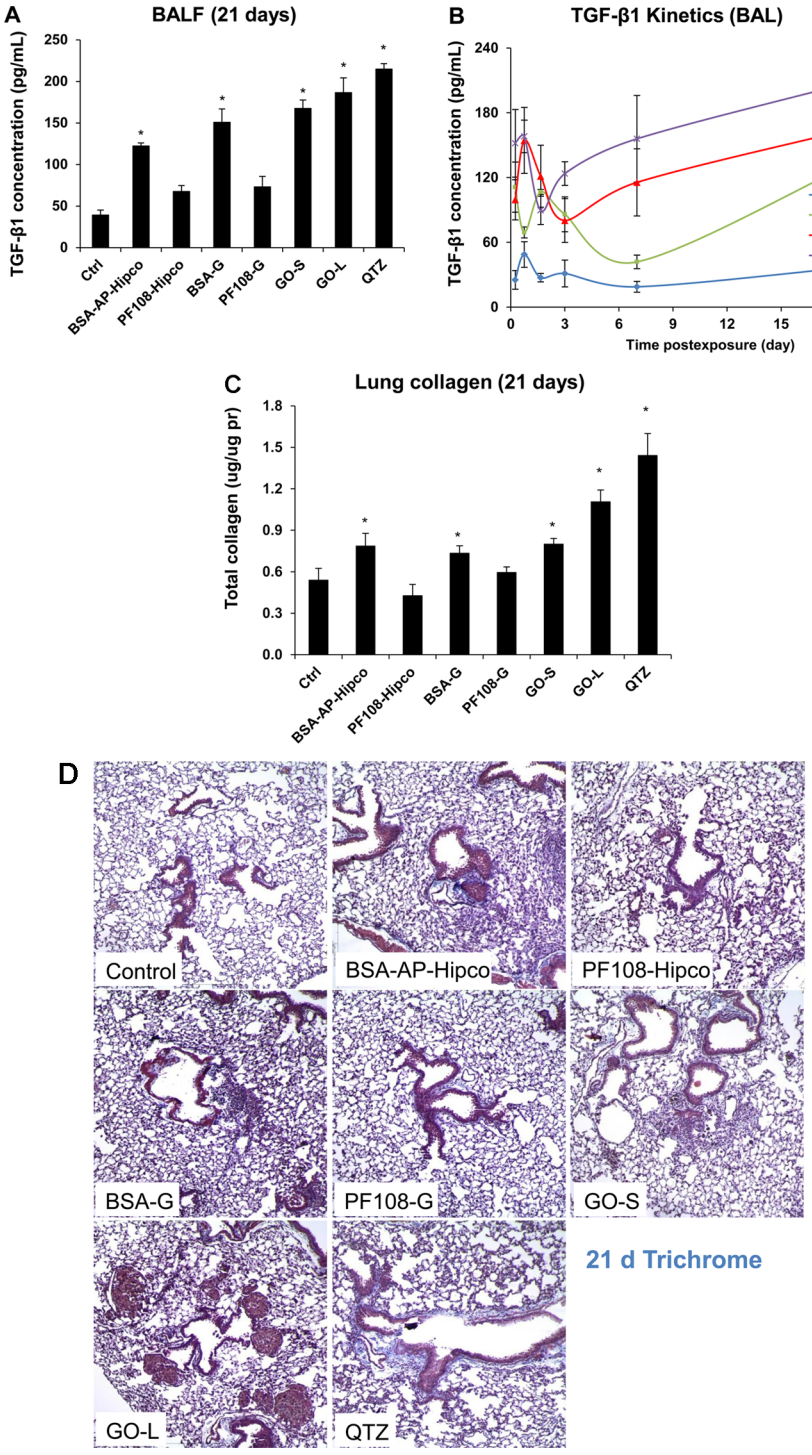

Figure 5. Comparison of the fibrogenic effects of ECNs in a subchronic oropharyngeal installation study. The experiment described in Figure 4A was repeated, except that the mice were sacrificed 21 days after oropharyngeal aspiration of Hipco-SWCNTs, graphene and GO at 2 mg/kg ($n = 6$ animals per group). The BALF was collected to determine TGF-β1 (A) levels. We also used the BALF collected from the kinetics experiment described in Figure 4B to measure the TGF-β1 (B) levels. *$p < 0.05$ compared to control. (C) Total lung collagen in the 21 d experiment, using the Sircol soluble collagen kit (Biocolor Ltd., Carrickfergus, U.K.). *$p < 0.05$ compared to control. (D) Collagen deposition in the lung as determined by Masson's trichrome staining. Lung tissues from (C) were embedded, sectioned, and stained with the Masson's trichrome. These lung images, shown at 100× magnification, are representative of the findings in each group. The blue staining represents collagen staining. Min-U-Sil exposed animals served as a positive control.

be triggered by different levels of metal impurities. These include the presence of iron (Fe) in Hipco SWCNT's, Ni in Arc and Co in CoMoCAT SWCNTs. These metals have been shown to play a role in ROS generation, cytotoxicity and pro-inflammatory outcomes by non-lysosomal pathways.[20−23]

Graphene is a two-dimensional (2D) material that is currently being explored in a variety of possible biomedical applications.[24−27] It is of interest that BSA-coated graphene poses the same hazard potential as one-dimensional SWCNTs, in spite of the differences in shape, size, aspect ratio, and metal content.[5,17] Although we lack a clear understanding of the earliest mechanism of biological injury by graphene, this report demonstrates that the graphene surface, similar to SWCNTs and MWCNTs, is capable of triggering lysosomal injury and participating in a final common AOP that culminates in pulmonary fibrosis. Decreased engagement of this AOP by PF108 coating of the graphene surface likely reflects dampening of the epoxide, carboxyl, and hydroxyl groups on the reactive GO surface. These groups are capable of oxygen radical generation, which could contribute to the lysosome damage and activation of NLRP3 inflammasome, similar to MWCNTs and SWCNTs.[28] In addition to surface reactivity, the size of the graphene flakes is important, as shown by the enhanced impact of larger flake surfaces capable of triggering IL-1β production and pulmonary fibrosis. These data are in agreement with previous findings showing that GO is more injurious than graphene in the lung, whether introduced intratracheally or intravenously.[5,29−31] A further important feature of GO is the hydrophilicity and aqueous stability of this material from the perspective that these features facilitate the razor-like morphology of GO flakes, enabling them to slip through the cell membrane and entering subcellular structures like lysosomes.[32] This could explain why the GO flakes with larger surface dimensions could speed up the kinetics of IL-1β production in the lung, in addition to stimulating more organ fibrosis. It has also been demonstrated previously that the size of GO flakes determines multivalent interactions between the functionalized surface and Toll-like receptors on the cell surface.[33] The hydrophilicity of GO flakes and their good dispersion may also allow deeper and more homogeneous distribution in the lung, compared to SWCNTs and pristine graphene.[5,31]

An important outcome of this study is the ability to achieve toxicological ranking of a diverse set of ECNs based on an AOP that is involved in the pathophysiology of disease. The capacity to compare large numbers of materials according to a common predictive toxicological paradigm holds great promise for expedited ranking of ECNs, which can then be used for categorization as well as integrative decision-making. Because of a growing interest in multiwall and single-wall CNTs as well as graphene for industrial and biomedical applications, it is likely that increased commercialization will intensify the need to make decisions on whether these materials are safe to enter the marketplace. Currently, for regulatory purposes, each nanomaterial is treated on a case by case basis, which could lead to unnecessary duplication of effort toward safety assessment. For inhaled materials, such as CNTs, current regulations could require a 90 day inhalation study, which could be very expensive and difficult to accomplish for a large number of materials. Our use of a predictive toxicological paradigm, which can be implemented by rapid throughput methodology based AOP that can be assessed in cells and easily confirmed by short-term bonus instillation studies in the rodent lung, could be used for a tiered testing paradigm that could replace the 90-day inhalation study (Figure 6). Thus, screening of pro-fibrogenic responses in epithelial cells and macrophages could allow newly introduced ECNs to undergo expedited testing against a library of previously screened materials (such as the one shown here) to obtain a provisional Tier 1 hazard ranking. If the new material demonstrates significant hazard potential in a Tier 1 assay, coupled with information on possible inhalation exposure in humans, it would be possible to perform a short-term bolus instillation (Tier 2) study, which should include positive and negative control materials to confirm or refute the *in vitro* prediction. If the short-term aspiration study confirms the hazard potential, this could help to justify the performance of a 90 day installation study (Tier 3) when significant uncertainty exists of how a new ECN may perform under aerosolized inhalation conditions. Hopefully, this scenario will only be used sparingly in light of the costs and the labor intensity of an inhalation study. We propose that the iterative use of a tiered approach will, over time, provide the incremental knowledge and data to allow acceptance, validation and incremental shift toward using *in vitro* approaches with sparing use of animals. Such an approach will also allow the assembly of libraries of ECN materials in which accentuation of certain properties such as CNT length, aspect ratio, surface functionality, surface coatings, surface defects, impurities, chirality, electronic properties, and defects can be introduced to allow the development of more detailed quantitative SARs and categorization. Such a knowledge base could have an important impact on regulatory decision-making, and safer design of ECNs, as demonstrated by the use of ECN surface coating with PF108.

CONCLUSION

In this study, we compared diverse ECNs for their ability to engage in pro-fibrogenic responses at the cellular level and culminating in pulmonary fibrosis. We demonstrate that the reactive surface of the ECNs is the primary physicochemical characteristic in this mechanistic paradigm, which can help predict the materials that are likely to trigger pro-fibrogenic responses *in vitro* and *in vivo*. This establishes an AOP that can be used for hazard ranking and setting up a tiered decision-making process for additional *in vivo* testing.

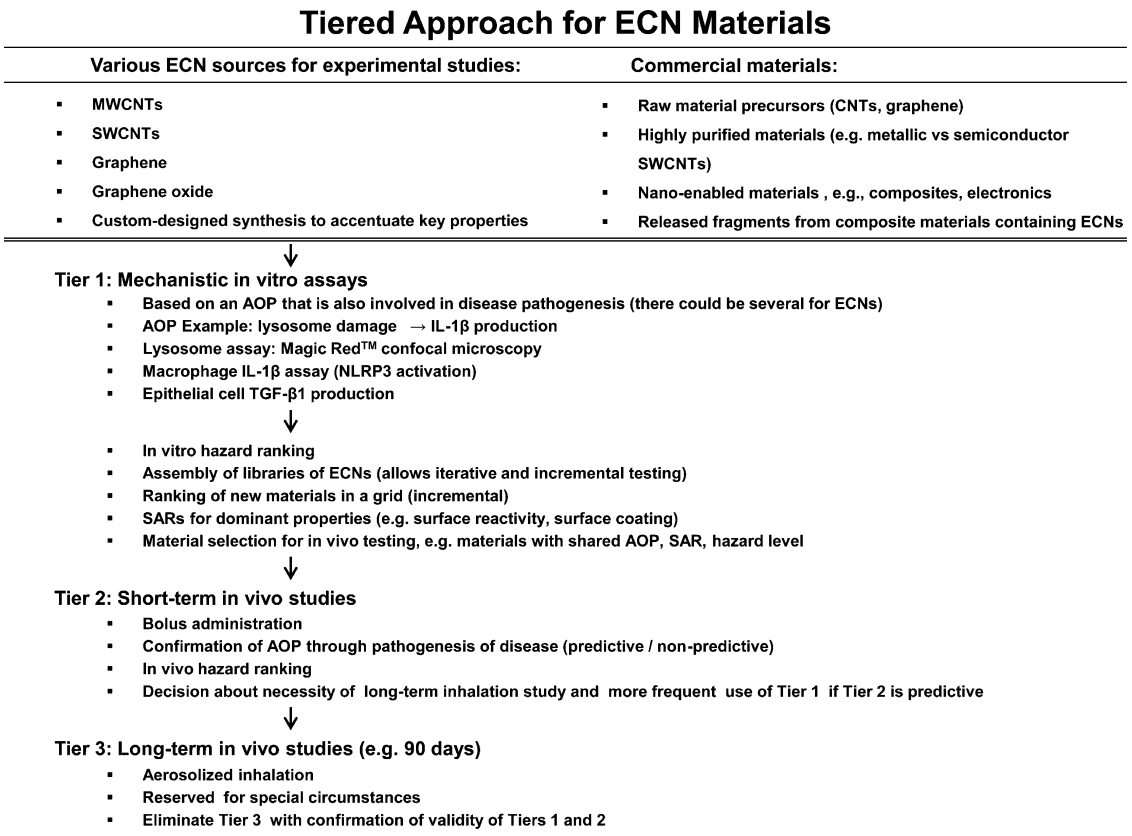

Figure 6. Outline of a possible tiered testing approach, according to which decision analysis can be developed for safety assessment of broad groups of ECNs, with a view to expediting testing, and regulatory decision-making.

PF108 coating is capable of passivating reactive ECN surfaces, which prevents lysosomal damage, NLRP3 inflammasome activation, IL-1β production and lung fibrosis.

MATERIALS AND METHODS

Source and Preparation of Carbonaceous Nanomaterials. We used SWCNTs prepared by three different methods. As-prepared (AP) and purified (PD) HiPco SWCNTs were purchased from Nano-Integris (Skokie, IL). AP- and PD-Arc-discharge SWCNTs were purchased from Carbon Solutions, Inc. (Riverside, CA). PD-CoMoCat (PD-SG65) SWCNTs were purchased from Southwest Nano Technologies (Norman, OK). Pluronic F108 (BASF Corporation, Iselin, NJ) dispersed SWCNTs (Hipco, Arc and CoMoCat) were prepared by sonicating the purified grade materials in 2% (w/v) PF108, followed by centrifugation to remove large aggregates and impurities as described previously.[17] PF108-dispersed graphene (PF108-G) was produced by ultrasonication of graphite flakes (3061 grade material from Asbury Graphite Mills) in a 2% aqueous PF108 solution, followed by centrifugation at ~4620*g* for 30 min to remove large flakes. Subsequent ultracentrifugation at 288000*g* for 12 h was used to concentrate and further purify the solution. Aggregated graphene was produced by flocculation though the addition of four parts isopropyl alcohol to one part dispersed graphene, followed by extensive washing in deionized water. Graphene oxide (GO) was produced *via* a modified Hummer's method from Asbury Mills 3061 grade graphite.[34] After oxidation, samples were washed *via* filtration and centrifugation. Small-sized GO (GO-S) was produced by horn sonication of the washed material, using a Fisher Scientific Model 500 Sonic Dismembrator, fitted with a 1/2 in. tip. Sonication was carried out at ~55 W (50% amplitude) in an ice bath for 1 h. Large-sized GO (GO-L) was produced by bath sonication for 1 h. Both GO-S and GO-L were subsequently centrifuged for 30 min in a Beckman Coulter J26-XPI at 5000 rpm (~4620*g*) to remove large aggregates. The top 80% of the supernatant was taken off as the final use material.

Chemicals and Experimental Materials. Bronchial epithelial growth medium (BEGM) was obtained from Lonza (Mapleton, IL). BEGM is supplemented with a number of growth factors, including bovine pituitary extract, insulin, hydrocortisone, hEGF, epinephine, triiodothyronine, transferrin, gentamicin/amphotericin-B and retinoic acid. Roswell Park Memorial Institute medium 1640 (RPMI 1640) was purchased from Invitrogen (Carlsbad, CA, USA). Low-endotoxin bovine serum albumin (BSA) and fetal bovine serum (FBS) were from Gemini Bio-Products (West Sacramento, CA). Dipalmitoylphosphatidylcholine (DPPC) was purchased from Sigma-Aldrich (St. Louis, MO). Min-U-Sil was obtained from U.S. Silica (Frederick, MD). All the SWCNT, graphene or graphene oxide stock solutions were prepared using pure deionized water (DI H_2O) with resistivity >18 Ω cm.

Preparation of Nanoparticle Suspensions. For BSA/DPPC dispersal, both dispersants were added at 0.6 and 0.01 mg/mL, respectively, before adding a 5 mg/mL ECN stock solution. To obtain highly dispersed PF108 tubes, ~33 mg of powder was added to 12 mL of 2% (w/v) PF108 aqueous solution, before sonication with a Fisher Scientific Model 500 Scientific Dismembrator for 1 h at 20% amplitude. These tubes were subsequently centrifuged at 32000*g* for 30 min, and the supernatants were retained as the PF108 dispersed stock solution.

Cell Culture and Co-incubation with SWCNT, Graphene and GO. BEAS-2B and THP-1 cells were obtained from ATCC (Manassas, VA). A total of 1×10^4 BEAS-2B cells were cultured in 0.1 mL BEGM in 96-well plates at 37 °C. THP-1 cells were pretreated with

1 μg/mL phorbol 12-myristate acetate (PMA) overnight and primed with 10 ng/mL lipopolysaccharide (LPS). Aliquots of 3×10^4 primed cells were cultured in 0.1 mL medium with carbon nanoparticles in 96-well plates (Costar, Corning, NY) at 37 °C for 24 h. All the carbon nanoparticle suspensions were freshly prepared. After 24 h of culture, the supernatants were collected for the measurement of IL-1β (BD Biosciences, San Diego, CA) and TGF-β1 (Promega, Madison, WI) using ELISA kits according to manufacturer's instructions. Concentrations were expressed as picograms per milliliter (pg/mL).

Confocal Microscopy Using Magic Red To Assess Lysosomal Damage and Cathepsin B Release. A total of 1×10^5 primed THP-1 cells were seeded into each well of an 8-well chamber and incubated with 100 μg/mL SWCNTs, graphene or GO flakes in RPMI 1640 for 4 h. After fixation in 4% paraformaldehyde for 1 h in PBS, cells were washed three times with PBS and stained with Magic Red (ImmunoChemistry Technologies) at 26 nM for 1 h. Following further washes with PBS, the cell membrane and nucleus were costained for 30 min with 5 μg/mL Alexa Fluor633-conjugated wheat germ agglutinin (WGA) and Hoechst 33342, respectively. The chamber was visualized under a confocal microscope (Leica Confocal 1P/FCS) in the CNSI Advanced Light Microscopy/Spectroscopy Shared Facility. High magnification images were obtained with the 100× objective. Cells without nanoparticle treatment were used as control. Cells treated with 100 μg/mL monosodium urate (MSU) crystals as the positive control.

Mouse Exposure and Assessment of Exposure Outcomes. Eight-week-old male C57Bl/6 mice were purchased from Charles River Laboratories (Hollister, CA). All animals were housed under standard laboratory conditions according to UCLA guidelines for care and treatment as well as the NIH Guide for the Care and Use of Laboratory Animals in Research (DHEW78-23). The animal experiments were approved by the Chancellor's Animal Research Committee at UCLA and include standard operating procedures for animal housing (filter-topped cages; room temperature at 23 ± 2 °C; 60% relative humidity; 12 h light, 12 h dark cycle) and hygiene status (autoclaved food and acidified water). Animal exposures to nanoparticles were carried out by an oropharyngeal aspiration method developed at NIOSH.[35] Briefly, the animals were anesthetized by intraperitoneal injection of ketamine (100 mg/kg)/xylazine (10 mg/kg) in a total volume of 100 μL. With the anesthetized animals held in a vertical position, a 50 μL PBS suspension containing 50 μg nanoparticles was instilled at the back of the tongue to allow pulmonary aspiration. The experiment included control animals receiving the same volume of PBS with BSA (0.6 mg/mL) and DPPC (0.01 mg/mL). The positive control group in each experiment received 5 mg/kg crystalline silica in the form of quartz (Min-U-Sil or QTZ). We performed two kinds of animal experiments, namely a study in which SWCNT, graphene and GO were compared for lung fibrosis potential, as well as performing a kinetics study in which the animals were observed for various lengths of time following oropharyngeal instillation. The mice in the comparison experiments were sacrificed at 40 h and 21 days postexposure, while the mice in the kinetics study were sacrificed at 6 h, 18 h, 40 h, 3 d, and 7 d postexposure. The bronchoalveolar lavage fluid (BALF) and lung tissues from each experiment were collected as previously described.[36] The BALF was used for performance of total and differential cell counts and the measurement of IL-1β and TGF-β1 levels. Lung tissues were stained with hematoxylin/eosin or Masson's trichrome.

Sircol Assay To Assess Total Collagen Production. The right upper lobe of each lung was suspended in PBS at ~50 mg tissue per ml and homogenized with a tissue homogenizer (Fisher Scientific). Triton X-100 was added at 1% and the samples incubated for 18 h at room temperature. Acetic acid was added to a final of 0.5 M and incubated at room temperature for 90 min. Cellular debris was pelleted by centrifugation, and the supernatants were used to assess total protein, using a BCA Assay kit (Pierce/ThermoFisher Scientific). The Sircol Soluble Collagen Assay kit (Biocolor Ltd., Carrickfergus, U.K.) was used to extract collagen from duplicate samples, using 200 μL of supernatant and 800 μL of Sircol Dye Reagent according to the manufacturer's instructions. Similar prepared collagen standards (10−50 μg) were run in parallel. Collagen pellets were washed twice with alcohol and dried before suspension in an alkaline reagent. Absorbance at 540 nm was read on a plate reader (SpectroMax M5e, Molecular Devices Corp., Sunnyvale, CA). Data were expressed as micrograms of soluble collagen per milligrams of total protein.

Statistical Analysis. Mean and standard deviation (SD) was calculated for each parameter. Results were expressed as mean ± SD of multiple determinations. Comparisons within each group were conducted by a two-sided Student's *t* test. A statistically significant difference was assumed with $p < 0.05$.

Conflict of Interest: The authors declare no competing financial interest.

Acknowledgment. Research reported in this publication was supported by the National Institute of Environmental Health Sciences of the National Institutes of Health under Award Number RO1ES022698 and U19ES019528. The content is solely the responsibility of the authors and does not necessarily represent the official views of the National Institutes of Health. This study is also based upon work supported by the National Science Foundation and the Environmental Protection Agency under Award No. DBI-1266377. Fluorescent microscopy was performed at the CNSI Advanced Light Microscopy/Spectroscopy Shared Facility at UCLA.

Supporting Information Available: Cell viability, suspension stability, *in vitro* cell uptake, *in vivo* cytokine production at 40 h and 21 d, neutrophil count, H&E staining. This material is available free of charge *via* the Internet at http://pubs.acs.org.

REFERENCES AND NOTES

1. Shvedova, A. A.; Kisin, E.; Murray, A. R.; Johnson, V. J.; Gorelik, O.; Arepalli, S.; Hubbs, A. F.; Mercer, R. R.; Keohavong, P.; Sussman, N.; et al. Inhalation *vs* Aspiration of Single-Walled Carbon Nanotubes in C57BL/6 Mice: Inflammation, Fibrosis, Oxidative Stress, and Mutagenesis. *Am. J. Physiol.: Lung Cell. Mol. Physiol.* **2008**, *295*, L552–L565.
2. Shvedova, A. A.; Kisin, E. R.; Mercer, R.; Murray, A. R.; Johnson, V. J.; Potapovich, A. I.; Tyurina, Y. Y.; Gorelik, O.; Arepalli, S.; Schwegler-Berry, D.; et al. Unusual Inflammatory and Fibrogenic Pulmonary Responses to Single-Walled Carbon Nanotubes in Mice. *Am. J. Physiol.: Lung Cell. Mol. Physiol.* **2005**, *289*, L698–L708.
3. Wang, X.; Xia, T.; Ntim, S. A.; Ji, Z.; Lin, S.; Meng, H.; Chung, C.; George, S.; Zhang, H.; Wang, M.; et al. Dispersal State of Multi-Walled Carbon Nanotubes Elicits Pro-Fibrogenic Cellular Responses that Correlate with Fibrogenesis Biomarkers and Fibrosis in the Murine Lung. *ACS Nano* **2011**, *5*, 9772–9787.
4. Warheit, D. B.; Laurence, B. R.; Reed, K. L.; Roach, D. H.; Reynolds, G. A. M.; Webb, T. R. Comparative Pulmonary Toxicity Assessment of Single-Wall Carbon Nanotubes in Rats. *Toxicol. Sci.* **2004**, *77*, 117–125.
5. Duch, M. C.; B, G. R.; Liang, Y. T.; Soberanes, S.; Urich, D.; Chiarella, S. E.; Campochiaro, L. A.; Gonzalez, A.; Chandel, N. S.; Hersam, M. C.; et al. Minimizing Oxidation and Stable Nanoscale Disperson Improves the Biocompatibility of Graphene in the Lung. *Nano Lett.* **2011**, *11*, 5201–5207.
6. Seabra, A. B.; Paula, A. J.; de Lima, R.; Alves, O. L.; Duran, N. Nanotoxicity of Graphene and Graphene Oxide. *Chem. Res. Toxicol.* **2014**, *27*, 159–168.
7. Bianco, A. Graphene: Safe or Toxic? The Two Faces of the Medal. *Angew. Chem., Int. Ed.* **2013**, *52*, 4986–4997.
8. Ma-Hock, L.; Strauss, V.; Treumann, S.; Kuttler, K.; Wohlleben, W.; Hofmann, T.; Groters, S.; Wiench, K.; van Ravenzwaay, B.; Landsiedel, R. Comparative Inhalation Toxicity of Multi-Wall Carbon Nanotubes, Graphene, Graphite Nanoplatelets and Low Surface Carbon Black. *Part. Fibre Toxicol.* **2013**, *10*.
9. Kayat, J.; Gajbhiye, V.; Tekade, R. K.; Jain, N. K. Pulmonary Toxicity of Carbon Nanotubes: A Systematic Report. *Nanomedicine* **2011**, *7*, 40–49.
10. Li, R. B.; Wang, X.; Ji, Z. X.; Sun, B. B.; Zhang, H. Y.; Chang, C. H.; Lin, S. J.; Meng, H.; Liao, Y. P.; Wang, M. Y.; et al. Surface Charge and Cellular Processing of Covalently

Functionalized Multiwall Carbon Nanotubes Determine Pulmonary Toxicity. *ACS Nano* **2013**, *7*, 2352–2368.
11. Wang, X.; Xia, T.; Duch, M. C.; Ji, Z. X.; Zhang, H. Y.; Li, R. B.; Sun, B. B.; Lin, S. J.; Meng, H.; Liao, Y. P.; et al. Pluronic F108 Coating Decreases the Lung Fibrosis Potential of Multiwall Carbon Nanotubes by Reducing Lysosomal Injury. *Nano Lett.* **2012**, *12*, 3050–3061.
12. Wang, X.; Xia, T.; Ntim, S. A.; Ji, Z. X.; George, S.; Meng, H.; Zhang, H.; Castranova, V.; Mitra, S.; Nel, A. E. Quantitative Techniques for Assessing and Controlling the Dispersion and Biological Effects of Multiwalled Carbon Nanotubes in Mammalian Tissue Culture Cells. *ACS Nano* **2010**, *4*, 7241–7252.
13. Sun, B. B.; Wang, X.; Ji, Z. X.; Li, R. B.; Xia, T. NLRP3 Inflammasome Activation Induced by Engineered Nanomaterials. *Small* **2013**, *9*, 1595–1607.
14. Bonner, J. C. Mesenchymal Cell Survival in Airway and Interstitial Pulmonary Fibrosis. *Fibrog. Tissue Repair* **2010**, *3*, 15.
15. Seo, J. W. T.; Green, A. A.; Antaris, A. L.; Hersam, M. C. High-Concentration Aqueous Dispersions of Graphene Using Nonionic, Biocompatible Block Copolymers. *J. Phys. Chem. Lett.* **2011**, *2*, 1004–1008.
16. Antaris, A. L.; Seo, J. W. T.; Green, A. A.; Hersam, M. C. Sorting Single-Walled Carbon Nanotubes by Electronic Type Using Nonionic, Biocompatible Block Copolymers. *ACS Nano* **2010**, *4*, 4725–4732.
17. Mutlu, G. M.; Budinger, G. R. S.; Green, A. A.; Urich, D.; Soberanes, S.; Chiarella, S. E.; Alheid, G. F.; McCrimmon, D. R.; Szleifer, I.; Hersam, M. C. Biocompatible Nanoscale Dispersion of Single-Walled Carbon Nanotubes Minimizes *in vivo* Pulmonary Toxicity. *Nano Lett.* **2010**, *10*, 1664–1670.
18. Liu, Y.; Zhao, Y. L.; Sun, B. Y.; Chen, C. Y. Understanding the Toxicity of Carbon Nanotubes. *Acc. Chem. Res.* **2013**, *46*, 702–713.
19. Ge, C. C.; Meng, L.; Xu, L. G.; Bai, R.; Du, J. F.; Zhang, L. L.; Li, Y.; Chang, Y. Z.; Zhao, Y. L.; Chen, C. Y. Acute Pulmonary and Moderate Cardiovascular Responses of Spontaneously Hypertensive Rats after Exposure to Single-Wall Carbon Nanotubes. *Nanotoxicology* **2012**, *6*, 526–542.
20. Fubini, B.; Ghiazza, M.; Fenoglio, I. Physico-Chemical Features of Engineered Nanoparticles Relevant to Their Toxicity. *Nanotoxicology* **2010**, *4*, 347–363.
21. Fubini, B.; Fenoglio, I.; Tomatis, M.; Turci, F. Effect of Chemical Composition and State of the Surface on the Toxic Response to High Aspect Ratio Nanomaterials. *Nanomedicine* **2011**, *6*, 899–920.
22. Shvedova, A. A.; Kisin, E. R.; Porter, D.; Schulte, P.; Kagan, V. E.; Fadeel, B.; Castranova, V. Mechanisms of Pulmonary Toxicity and Medical Applications of Carbon Nanotubes: Two Faces of Janus? *Pharmacol. Ther.* **2009**, *121*, 192–204.
23. Kagan, V.; Potapovich, A.; Osipov, A.; Schwegler-Berry, D.; Kisin, E.; Mercer, R.; Castranova, V.; Shvedova, A. Iron-Rich Single Walled Carbon Nanotubes Are Effective Catalysts of Oxidative Stress in Raw 264.7 Macrophage Cell Culture Model: Interactions with Inflammatory Response and *in Vivo* Implications. *Free Radical Biol. Med.* **2004**, *37*, S51–S52.
24. Kostarelos, K.; Novoselov, K. S. Exploring the Interface of Graphene and Biology. *Science* **2014**, *344*, 261–263.
25. Feng, L. Z.; Liu, Z. A. Graphene in Biomedicine: Opportunities and Challenges. *Nanomedicine* **2011**, *6*, 317–324.
26. Hung, A. H.; Holbrook, R. J.; Rotz, M. W.; Glasscock, C. J.; Mansukhani, N. D.; MacRenaris, K. W.; Manus, L. M.; Duch, M. C.; Dam, K. T.; Hersam, M. C.; et al. Graphene Oxide Enhances Cellular Delivery of Hydrophilic Small Molecules by Co-Incubation. *ACS Nano* **2014**, *8*, 10168–10177.
27. Hung, A. H.; Duch, M. C.; Parigi, G.; Rotz, M. W.; Manus, L. M.; Mastarone, D. J.; Dam, K. T.; Gits, C. C.; MacRenaris, K. W.; Luchinat, C.; et al. Mechanisms of Gadographene-Mediated Proton Spin Relaxation. *J. Phys. Chem. C* **2013**, *117*, 16263–16273.
28. Das, S.; Singh, S.; Singh, V.; Joung, D.; Dowding, J. M.; Reid, D.; Anderson, J.; Zhai, L.; Khondaker, S. I.; Self, W. T.; et al. Oxygenated Functional Group Density on Graphene Oxide: Its Effect on Cell Toxicity. *Part. Part. Syst. Charact.* **2013**, *30*, 148–157.
29. Zhang, X. Y.; Yin, J. L.; Peng, C.; Hu, W. Q.; Zhu, Z. Y.; Li, W. X.; Fan, C. H.; Huang, Q. Distribution and Biocompatibility Studies of Graphene Oxide in Mice After Intravenous Administration. *Carbon* **2011**, *49*, 986–995.
30. Liu, J. H.; Wang, T. C.; Wang, H. F.; Gu, Y. G.; Xu, Y. Y.; Tang, H.; Jia, G.; Liu, Y. F. Biocompatibility of Graphene Oxide Intravenously Administrated in Mice-Effects of Dose, Size and Exposure Protocols. *Toxicol. Res.* **2015**, *4*, 83–91.
31. Liu, J. H.; Yang, S. T.; Wang, H. F.; Chang, Y. L.; Cao, A. N.; Liu, Y. F. Effect of Size and Dose on the Biodistribution of Graphene Oxide in Mice. *Nanomedicine* **2012**, *7*, 1801–1812.
32. Li, Y. F.; Yuan, H. Y.; von dem Bussche, A.; Creighton, M.; Hurt, R. H.; Kane, A. B.; Gao, H. J. Graphene Microsheets Enter Cells Through Spontaneous Membrane Penetration at Edge Asperities and Corner Sites. *Proc. Natl. Acad. Sci. U.S.A.* **2013**, *110*, 12295–12300.
33. Qu, G. B.; Liu, S. J.; Zhang, S. P.; Wang, L.; Wang, X. Y.; Sun, B. B.; Yin, N. Y.; Gao, X.; Xia, T.; Chen, J. J.; et al. Graphene Oxide Induces Toll-Like Receptor 4 (TLR4)-Dependent Necrosis in Macrophages. *ACS Nano* **2013**, *7*, 5732–5745.
34. Chowdhury, I.; Duch, M. C.; Mansukhani, N. D.; Hersam, M. C.; Bouchard, D. Colloidal Properties and Stability of Graphene Oxide Nanomaterials in the Aquatic Environment. *Environ. Sci. Technol.* **2013**, *47*, 6288–6296.
35. Sun, B.; Wang, X.; Ji, Z.; Wang, M.; Liao, Y-P.; Chang, C. H.; Li, R.; Zhang, H.; Nel, A. E.; Xia, T. NADPH Oxidase-Dependent NLRP3 Inflammasome Activation and Its Important Role in Lung Fibrosis by Multiwalled Carbon Nanotubes. *Small* **2015**, DOI: 10.1002/smll.201402859.
36. Li, N.; Wang, M. Y.; Bramble, L. A.; Schmitz, D. A.; Schauer, J. J.; Sioutas, C.; Harkema, J. R.; Nel, A. E. The Adjuvant Effect of Ambient Particulate Matter Is Closely Reflected by the Particulate Oxidant Potential. *Environ. Health Perspect.* **2009**, *117*, 1116–1123.